Simulation of Flow Around Cylinder Actuated by DBD Plasma

WANG Yuling (王玉玲), GAO Chao (高超), WU Bin (武斌), HU Xu (胡旭)

National Key Laboratory of Science and Technology on Aerodynamic Design and Research, Northwestern Polytechnical University, Xi'an 710072, China

Abstract The electric-static body force model is obtained by solving Maxwell's electromagnetic equations. Based on the electro-static model, numerical modeling of flow around a cylinder with a dielectric barrier discharge (DBD) plasma effect is also presented. The flow streamlines between the numerical simulation and the particle image velocimetry (PIV) experiment are consistent. According to the numerical simulation, DBD plasma can reduce the drag coefficient and change the vortex shedding frequencies of flow around the cylinder.

Keywords: dielectric-barrier-discharge, plasma, body force, flow around cylinder

PACS: *52.25.Fi, 52.70.Nc, 52.75.Di, 52.80.Tn*

DOI: 10.1088/1009-0630/18/7/12

(Some figures may appear in colour only in the online journal)

1 Introduction

As a classical fluid mechanics problem, research of the flow around a circular cylinder has an important significance in theory [1−4]; it was widely used in engineering practice, and also the basic of other kinds of flow over a bluff body.

DBD plasma flow control, a new technology of active flow control, which uses plasma to induce atmospheric turbulence, is extremely suitable for the applications of flow control [5−8]. At the same time, it draws great attention both in industrial and academic circles [9]. Kolzlov [10] and Su [11] researched the plasma flow control around a cylinder. Hao [12] focused on applying the bipolar plasma actuator of flow around a circular cylinder. Ed Peers [13] investigated the plasma actuation applied on the surface of a bluff body using the velocity-inlet boundary condition. Suzen [14] and Li [15] numerically studied the model of the plasma flow control around a cylinder.

This work carried out the numerical simulations of the plasma control which were based on the experiments of the flow around a circular cylinder proposed by Kozlov. This paper solved simplified Maxwell electromagnetic equations, obtained the potential distribution and charge distribution of the DBD plasma actuator, established the electrostatic force model of DBD plasma body force [16], also developed the numerical simulation of DBD plasma flow control around a cylinder. The DBD plasma actuated on a cylinder or a plate had no essential difference, and both of the cases could make the air ionization and generate the body force by loading high frequency and high voltage through two electrodes. When the body force acted on the boundary layer, the flow field structure was thus changed. This work used the electrostatic force model in the numerical simulations of DBD plasma flow control, obtained the distribution of body force, and solved the flow equation with it. At last, we could get DBD plasma flow control around a cylinder.

2 Electrostatic force model of DBD plasma body force

Generally, the flow speed level is from 10 m/s to 100 m/s in engineering application research. While, in the process of plasma formation, the temperature of the electronic is 1000–10000 K, and the velocity will be 10^5–10^6 m/s. Based on the significant differences of the velocity levels, the plasma aerodynamic actuation is divided into two processes: the formation of body force and the response of the flow.

We assume that the plasma system is quasi static, then elementary current $\vec{j}$, magnetic strength $\vec{H}$, and magnetic induction intensity $\vec{B}$ will all become 0. Also, the time derivative is 0. So Maxwell's equations can be simplified into the following equations:

$$\nabla(\varepsilon\nabla\Phi) = -\frac{\rho_{\rm c}}{\varepsilon_0}, \tag{1}$$

where ε, Φ, $\rho_{\rm c}$, and ε_0 are the dielectric constant, potential, electric charge density, and dielectric constant in a vacuum, respectively.

For the weakly ionized gas particles, the potential can be assumed to consist of two parts which are respectively induced by the external electric field and the net charge density in the plasma, and we define them as ϕ and φ, separately; therefore,

$$\Phi = \phi + \varphi. \tag{2}$$

Assume that, if the charge is not large on the wall, meanwhile the Debye thickness is small, then the charged specie distribution in the domain is mainly governed by the potential resulting from electric charge on the wall but not the external electric field. Thus, two separate equations can be expressed in terms of the two aforementioned potentials, the first one arises due to the electric field induced by the external voltage at the electrodes:

$$\nabla \cdot (\varepsilon_{\mathrm{r}} \nabla \phi) = 0, \tag{3}$$

where ε_{r} is relative permittivity; the second one originates from the potential induced by the charged particles:

$$\nabla \cdot (\varepsilon_{\mathrm{r}} \nabla \varphi) = -\rho_{\mathrm{c}}/\varepsilon_0. \tag{4}$$

Introducing the Debye length, λ_{d}

$$\rho_{\mathrm{c}}/\varepsilon_0 = (-1/\lambda_{\mathrm{d}}^2)\varphi\,, \tag{5}$$

then, we can get the expression of the electric potential:

$$\varphi = -\rho_{\mathrm{c}}\lambda_{\mathrm{d}}^2/\varepsilon_0\,. \tag{6}$$

Substituting Eq. (6) into Eq. (4), an equation formed by the net charge density which can be at any point within the plasma is obtained.

$$\nabla \cdot (\varepsilon_{\mathrm{r}} \nabla \rho_{\mathrm{c}}) = \rho_{\mathrm{c}}/\lambda_{\mathrm{d}}^2\,. \tag{7}$$

Once we respectively obtain the values of ϕ and ρ_{c} from solving Eqs. (3) and (7), and meanwhile we neglect the magnetic forces. Then, the electrohydrodynamic force can be expressed as body force vector, that is

$$\vec{f}_{\mathrm{B}} = \rho_{\mathrm{c}}\vec{E} = -\rho_{\mathrm{c}}\nabla\Phi\,, \tag{8}$$

where $\vec{f}_{\mathrm{B}}$ is volume force per unit volume and $\vec{E}$ is electric field intensity vector.

As AC voltage is applied to the exposed (upper) electrode, the boundary condition can be written as:

$$\phi(t) = \phi^{\max} f(t)\,,$$

where $\phi(t)$ is upper electrode voltage and $\phi^{\max}$ is maximum voltage, and $f\ (t)$ is the wave form function, which is a sine wave denoted by $f(t) = \sin(2\pi wt)$.

If we assume that the electric potential on the embedded electrode is zero, and at the outer boundaries, $\frac{\partial\phi}{\partial n} = 0$, where n is normal direction, the net charge density is solved by Eq. (7), on the air side of the domain, considering ρ_{c}= 0 to use the boundary conditions. A zero normal gradient is imposed for the net charge density on the solid walls besides the region covering the lower electrode. On the region over the embedded electrode and downstream of the exposed electrode, the distribution of the charge density can be expressed by the following equation:

$$\rho_{\mathrm{c,w}}(x,t) = \rho_{\mathrm{c}}^{\max} G(x) f(t)\,, \tag{9}$$

where $\rho_{\mathrm{c,w}}(x,t)$, $\rho_{\mathrm{c}}^{\max}$ and $G(x)$ are the charge distribution at the top of the lower electrode, maximum charge density, and charge distribution, respectively.

It has been experimentally confirmed that the distribution mentioned above is analogous to the following expression which is a half Gaussian distribution:

$$G(x) = \exp[-(x-\mu)^2/(2\sigma^2)], \tag{10}$$

where $G(x)$ is based on the experience of the experiment, in general, the maximum value of $G(x)$ is in the leftmost side of the lower electrode. μ and σ are the maximum of the x location parameter and standard deviation, respectively. Meanwhile, they are also the scale parameters which determine the rate of decay. If the electrode size changes, the corresponding parameters μ and σ in the formula also need to be changed. In this computation, we choose $x = \mu$, $\sigma = 0.3$.

3 Calculation model and mesh generation

Calculation model is shown in Fig. 1, the selected model parameters are the same as in Kozlov's [3] experiment. The cylinder model is composed of a quartz glass cylinder (1), the outer diameter, wall thickness, and dielectric constant of which are $D = 100$ mm, $d = 2.5$ mm, and $\varepsilon = 3.7$, respectively. Fig. 1 shows the configuration, in which the cylinder wall acts as the dielectric barrier to obtain the SDBD plasma. Mounting the exposed electrodes to the surface of the cylinder, also their plasma generating edges located at $\pm45^{\mathrm{o}}$ and $\pm90^{\mathrm{o}}$ with respect to the approach flow direction. The arc distance between the 45^{o} and 90^{o} actuators is 12.5π mm (about 39.25 mm), which is far greater than the effect region of the actuator model. Therefore, the mutual influence between the two actuators can be ignored. The thickness and width of the copper foil electrodes (2) on the outer surface of the cylinder are 0.046 mm and 6.4 mm, respectively, and the corresponding four inner electrodes (3) made of lead foil are fixed on the inner surface of the cylinder (4) with thickness of 0.046 mm and width of 25.4 mm. In order to prevent inner discharge, the inner electrodes are covered by seven layers of Kapton tape with thickness of 0.889 mm, and the dielectric constant of the Kapton tape is 2.7. As shown in Fig. 1, each of the actuators is connected to a high voltage AC source which can generate a sinusoidal excitation of 11.4 kV at 10 kHz.

The velocity of free stream is 4 ± 0.3 m/s, cylinder diameter is 0.1 m, the Reynolds number is about $Re = 2.5\times10^4$, and the Karman Vortex Street appears alternately in the rear of the Cylindrical. As the flow velocity, the characteristic length of the model, and the kinematic viscosity are known, then the Reynolds number can be calculated from the following equation:

$$Re = \frac{\rho V_\infty L}{\mu}. \tag{11}$$

The Reynolds number has an great influence on the flow around a cylinder. The calculated cylinder vortex

structures obtained from different Reynolds numbers are different. In order to compare with the results of the experiment, this paper aimed at the vortex structure of $Re = 2.5\times10^4$.

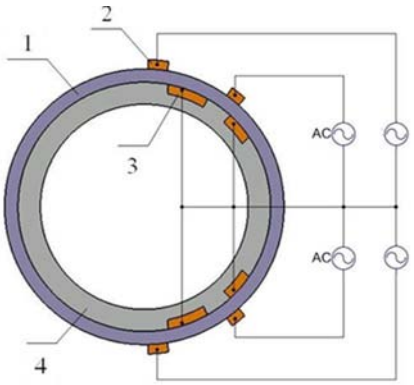

Fig.1 Schematic view of four SDBD plasma actuators fixed on the cylinder model [3]

In calculations, we used the ICEM CFD (Integrated Computer Engineering and Manufacturing code for Computational Fluid Dynamics) to generate a mesh of flow around a circular cylinder, where ICEM CFD was a software for grid division. The total meshes were about 4.7×10^5 , and the meshes were dense around electrodes, boundary layer, and the rear of the cylinder. In order to simulate the Karman vortex street, mesh refinement was used in the rear of the cylinder, as shown in Fig. 2. At the same time, we refine the mesh around the four actuators to calculate the induced body force.

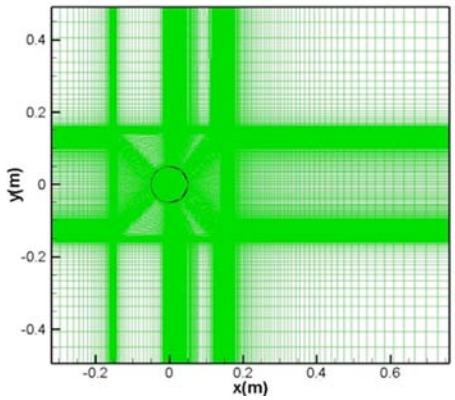

Fig.2 Grid division of flow around a circular cylinder

4 Results analysis

A potential of the external electric field ϕ was solved in the whole computational domain, Fig. 3(a)–(d) show the dimensionless distribution of external electric potential ϕ and the distribution of electric field lines, respectively. For four parallel actuators, electric field intensity directs from the high potential of the exposed electrode to the low potential of the embedded electrode. Near the gap of two electrodes, the electric potential gradient is larger, and directions of electric field lines originate from exposed electrodes, pointing to the embedded electrodes. In addition, there are also electric field lines from the exposed electrodes located at ±45° to the embedded electrodes located at ±90°.

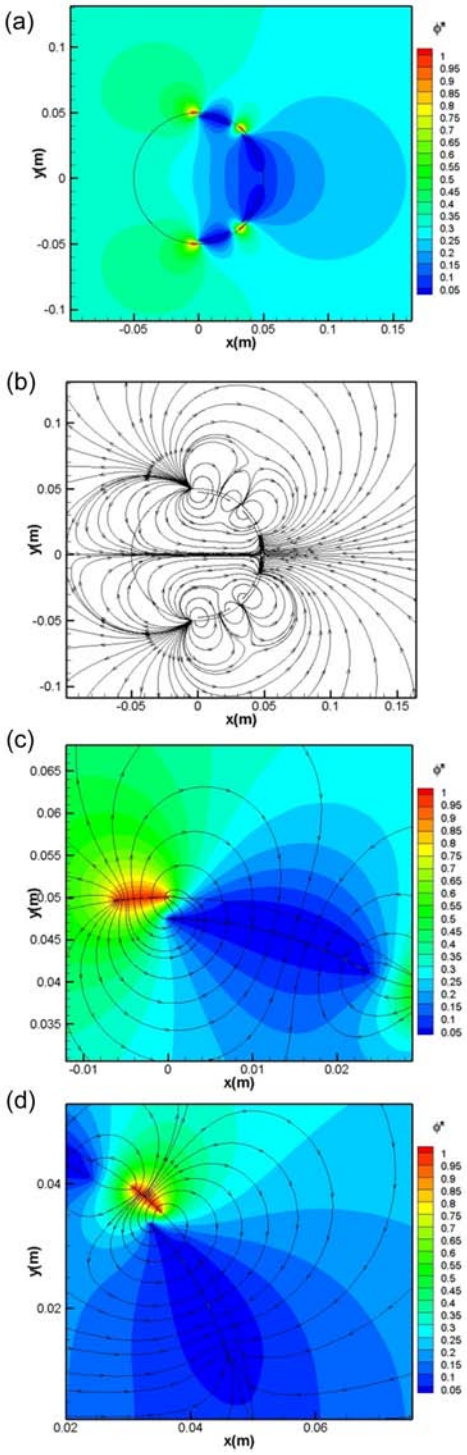

Fig.3 (a) The dimensionless distribution of electric potential, (b) Distribution of electric field lines, (c) The distribution of electric potential near electrodes located at ±90°, (d) Electric potential distribution near electrodes located at ±45°

Electric charged density equation solved in the whole air domain. Fig. 4(a) shows the distribution of the charge density around the cylinder. Fig. 4(b) and

Fig. 4(c) respectively show the charge density distribution of near electrodes located at ±45° and ±90°. It is observed that the electric charges concentrate in the top of embedded electrodes and the gap between two electrodes. The greatest density of electric charge is on the far left of the embedded electrode, and decreases gradually outward. About 2 mm from the wall, the electric charge density reduces to 5% of maximum. In a circumference direction, from left to right, electric charge density decreases sharply.

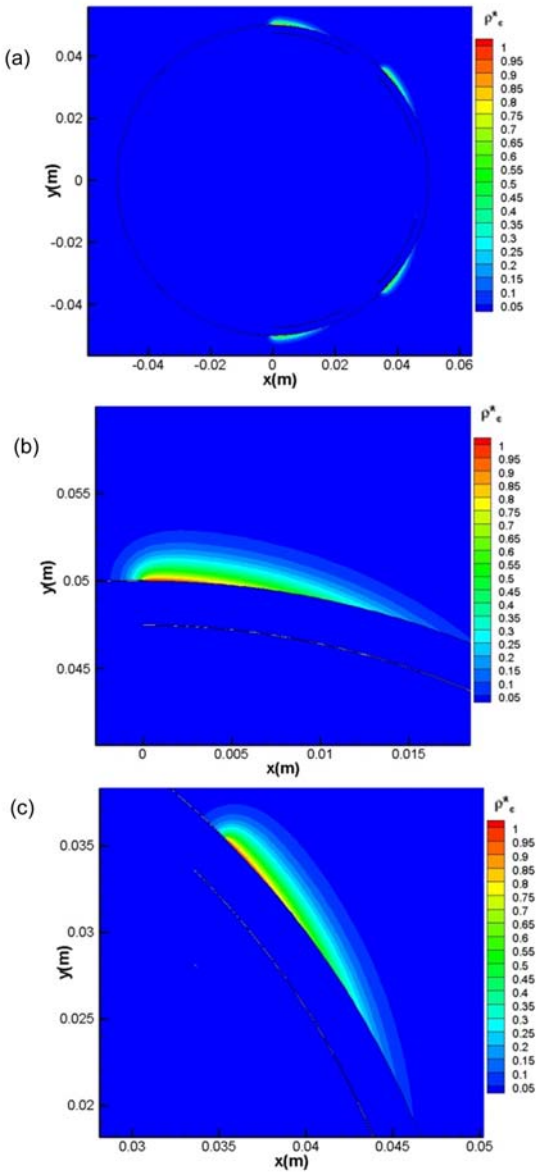

Fig.4 (a) The dimensionless distribution of the charge density, (b) The distribution of the charge density near actuators located at ±90°, (c) Charge density distribution near actuators located at ±45°

Fig. 5(a)–(d) respectively show the dimensionless distribution of the body force and vector near actuators located at ±90° and ±45°, which reach maximum in the gap of two electrodes, and decrease rapidly outward. The directions of body force vectors are the same as that of the electric field intensity.

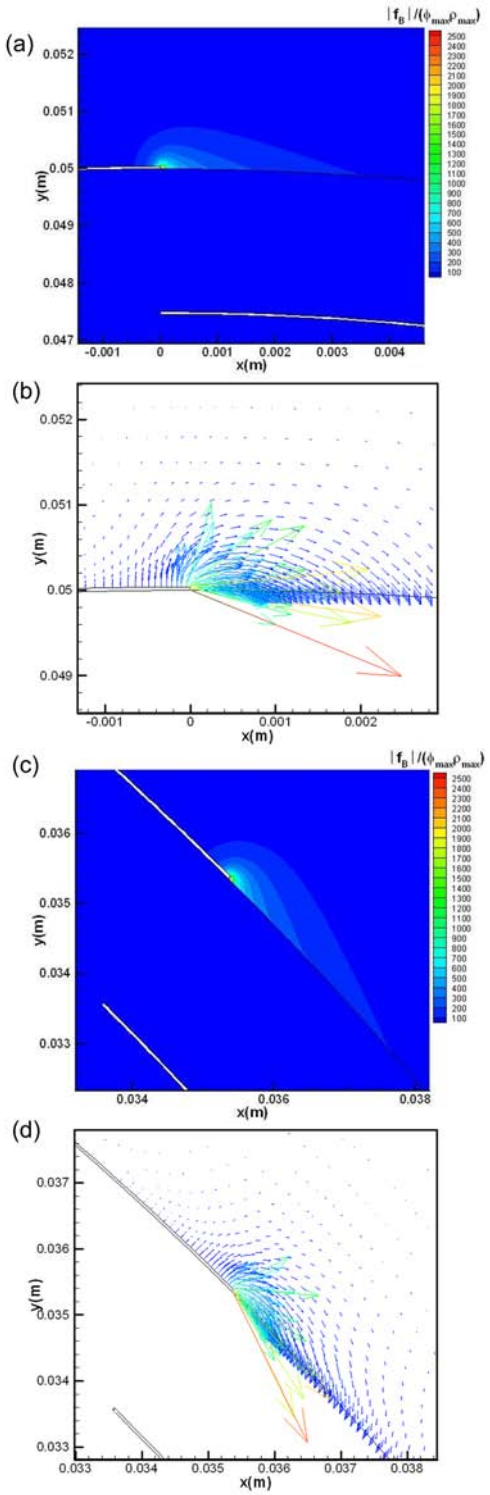

Fig.5 (a) The dimensionless distribution of the body force near actuators located at ±90°, (b) The distribution of the body force vector near actuators located at ±90°, (c) The dimensionless distribution of the body force near actuators located at ±45°, (d) The distribution of the body force vector near actuator located at ±45°

As it is indicated in some literatures [9], dimensionless frequency of flow around a cylinder is about 0.21,

$$Sr = 0.21 = \frac{f \times D}{U} = \frac{D}{TU}. \tag{12}$$

Take cylindrical model diameter $D = 0.1$ m, and incoming flow $U = 4$ m/s, it can be estimated that the period of vortex shedding $T = 0.119$ s. Meanwhile, the frequency of the DBD plasma actuator voltage $f = 10$ kHz, period is 0.0001 s, thus it is considered that the body force is steady. After time averaging, body force is taken as momentum source terms in to flow control equations to numerical simulation.

As cylinder diameter $D = 0.1$ m, take the cylindrical center as the reference, the computational domain is as follows: the left boundary is $6D$ from the center of the circle, as the velocity inlet; the right boundary is $16D$ from the center of the circle, as the outflow boundary. The upper and lower boundary is $5D$ from the center of the circle. To eliminate the influence of the wall, we use moving boundaries with velocity $U = 4$ m/s, and the turbulence model is the SST k-ω model.

Fig. 6 shows the vorticity distribution of the flow around a cylinder without plasma in $T/4$, $2T/4$, $3T/4$, and $4T/4$. In the given incoming flow conditions, the Karman Vortex Street is staggered distributed behind the cylinder.

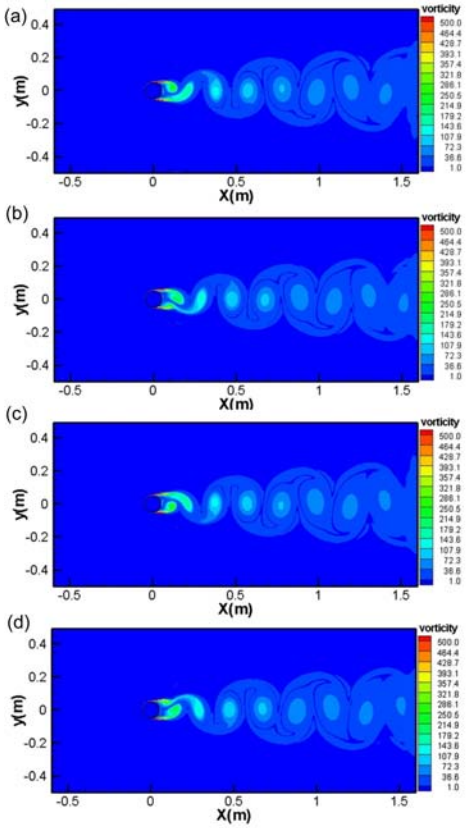

Fig.6 (a) Vorticity distribution without plasma in $T/4$, (b) Vorticity distribution without plasma in $2T/4$, (c) Vorticity distribution without plasma in $3T/4$, (d) Vorticity distribution without plasma in $4T/4$

Fig. 7 shows the vorticity distribution of the flow around a cylinder with plasma in $T/4$, $2T/4$, $3T/4$, and $4T/4$. In the given incoming flow condition, the Karman Vortex Street is also staggered distributed behind the cylinder, while different to the result of the no plasma situation.

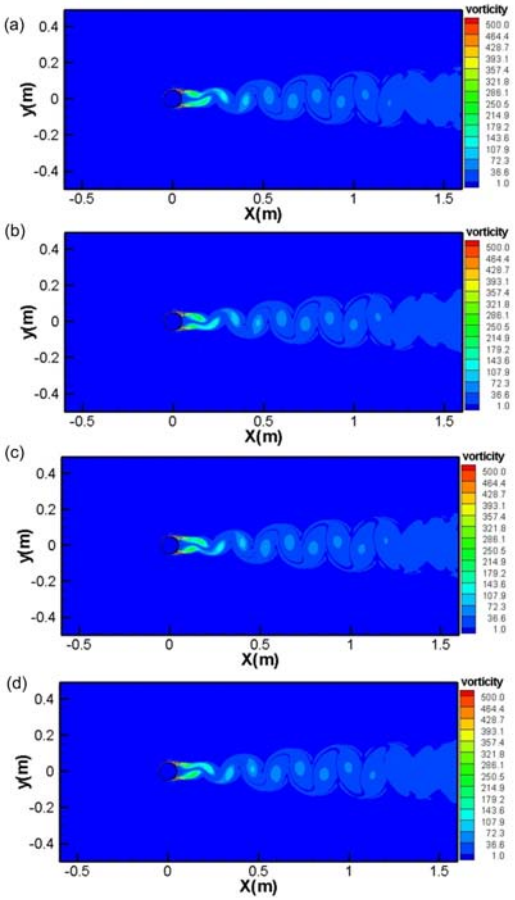

Fig.7 (a) Vorticity distribution with plasma in $T/4$, (b) Vorticity distribution with plasma in $2T/4$, (c) Vorticity distribution with plasma in $3T/4$, (d) Vorticity distribution with plasma in $4T/4$

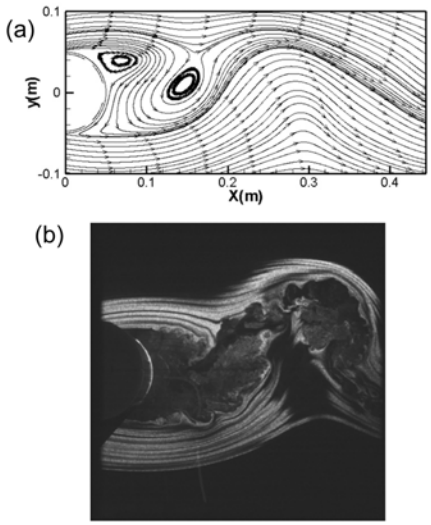

Fig.8 (a) The calculation result of the flow around a cylinder without plasma, (b) The PIV result of the flow around a cylinder without plasma [3]

Fig. 8(a) shows the calculation result of the flow field of the flow around a cylinder without plasma, and the PIV experiment result is shown in Fig. 8(b). Fig. 9(a) and (b) show the calculation result and PIV experiment result with plasma of the flow around a cylinder. It is observed that the calculation result is the same

as the PIV experiment result. There is a significant change of the structure of the flow around a cylinder with plasma, the vortex center is closer to the cylinder with plasma, one vortex is bigger and the other is smaller with plasma than that without plasma. It reduces the separation zone in the rear of the cylinder, and promotes re-circulation and the reattachment process.

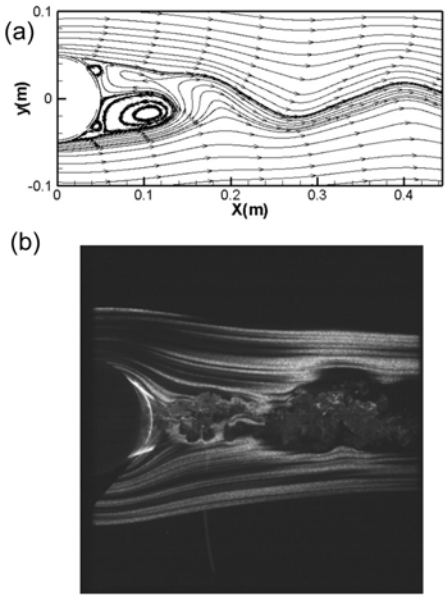

Fig.9 (a) The calculation result of the flow around a cylinder without plasma, (b) The PIV result of the flow around a cylinder without plasma [3]

Fig. 10 shows the over time change of lift coefficient of the flow around a cylinder. When the plasma is on, the maximum lift coefficient can rise to 0.064. On the other side, due to the plasma effect, flow separation is restrained and asymmetry is reduced, with the maximum of the lift coefficient reducing to 0.007.

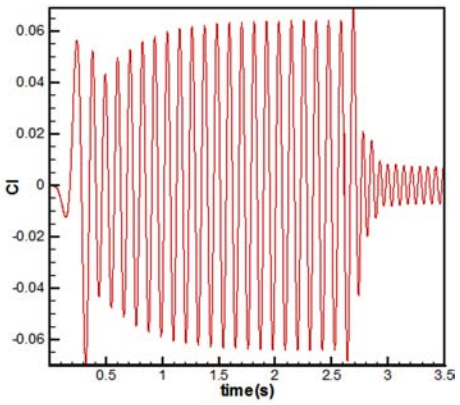

Fig.10 The change of lift coefficient of the flow around a cylinder

Fig. 11 shows the over time change of the drag coefficient of the flow around a cylinder with and without plasma. As the plasma is off, the average drag coefficient is 0.105. While the plasma is on, the separation zone of the rear cylinder is reduced, differential pressure also decreases, drag coefficient fluctuates over time in the range of 0.043-0.044, and the average value is 0.0435.

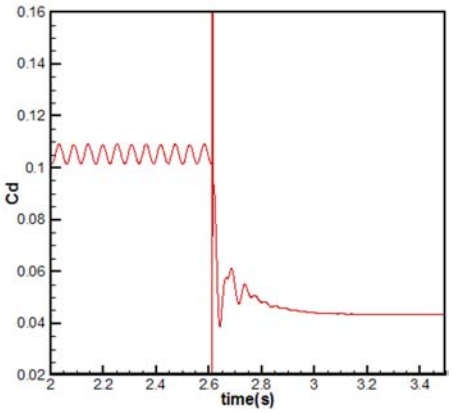

Fig.11 The over time change of drag coefficient of the flow around a cylinder

Due to the change of lift coefficient and drag coefficient, we can obtain that the period of vortex shedding is 0.11 s without plasma, but is 0.071 s with plasma. It can be concluded that plasma can help to reduce the drag coefficient and change the period of vortex shedding.

5 Conclusions

In this paper, we obtained the electric potential distribution and the charge distribution of DBD plasma via solving simplified Maxwell's electromagnetic equations. We established the electrostatic force model of the body force and carried out the numerical simulation of flow around a cylinder. The simulation results are consistent with the experimental results. As the plasma is off, the maximum of the lift coefficient, the average drag coefficient, and the period of vortex shedding are 0.064 s, 0.105 s, and 0.11 s, respectively. When the plasma is on, the maximum lift coefficient is 0.007, and the period of vortex shedding is 0.071 s; meanwhile, the drag coefficient fluctuates over time in the range of 0.043–0.044 with the average value of 0.0435. The numerical simulation showed that DBD plasma can reduce the drag coefficient of flow around a cylinder and change the frequency of vortex shedding, holding great promise for reducing drag and noise.

References

1 Yang Jiwei, Fu Xiaoli. 2008, China Water Transport, 8: 156 (in Chinese)
2 Catalano P, Wang M, Iaccarino G, et al. 2003, International Journal of Heat & Fluid Flow, 24: 463
3 Kozlov A V, Thomas F O. 2011, AIAA Journal, 49: 2183
4 Tabatabaeian S, Mirzaei M, Sadighzadeh A, et al. 2015, Journal of Applied Fluid Mechanics, 8: 291
5 Eid A, Takashima K, Mizuno A. 2014, IEEE Transactions on Industry Applications, 50: 4221

6 Wang J J, Choi K S, Feng L H, et al. 2013, Progress in Aerospace Sciences, 62: 52
7 Neretti G, Cristofolini A, Borghi C A, et al. 2012, IEEE Transactions on Plasma Science, 40: 1678
8 Corke T C, Enloe C L, Wilkinson S P. 2010, Annual Review of Fluid Mechanics, 42: 505
9 Nie Wansheng, Cheng Yufeng, Che Xueke. 2012, Advances in Mechanics, 42: 722 (in Chinese)
10 Alexey V Kozlov. 2010, Plasma Actuators for Bluff Body Flow Control [Ph.D]. The University of Notre Dame, Indiana
11 Su Changbin, Song Huimin, Li Yinghong. 2006, Journal of Experiments in Fluid Mechanic, 20: 45 (in Chinese)
12 Hao Jiangnan, Cai Jinsheng, Li Wenfeng. 2012, Journal of Experiments in Fluid Mechanic, 26: 11 (in Chinese)
13 Peers E, Huang X, Luo X. 2009, IEEE Transactions on Plasma Science, 37: 2250
14 Suzen Y B, Huang P G, Jacob J D, et al. 2005, Numerical Simulations of Plasma Based Flow Control Applications. 35th AIAA Fluid Dynamics Conference and Exhibit, Toronto, Ontario Canada, AIAA 2005-4633
15 Li Gang, Huang Weidong, Zhu Junqiang, et al. 2007, Journal of Aerospace Power, 22: 2073 (in Chinese)
16 Zhang Qunfeng, He Hongtao, Lv Ziyong. 2009, Science Technology and Engineering, 9: 1187 (in Chinese)

(Manuscript received 25 August 2015)
(Manuscript accepted 7 December 2015)
E-mail address of WANG Yuling:
wangyuling@nwpu.edu.cn